Phthalocyanine Nanoparticle Formation in Supersaturated Solutions

Edward Van Keuren,* Alysia Bone, and Changbao Ma

Department of Physics, Georgetown University, Washington, D.C. 20057

Received January 28, 2008. Revised Manuscript Received March 13, 2008

Self-organization of molecules in solution is an important natural and synthetic process, in particular for the preparation of nanomaterials. However, the mechanism of growth for solution-based nanoparticle formation is not always well understood. We present results that clarify these mechanisms in solutions of magnesium phthalocyanine in which the self-organization is induced by addition of a miscible nonsolvent. From simultaneous measurements of the sizes of the growing nanoparticles by photon correlation spectroscopy and the molecular concentration by absorption and fluorescence spectroscopy, we have found that the particles do not grow by molecular diffusion to the surfaces. These results suggest the importance of unstable clusters in the growth process. We also observed a strong dependence of the particle size on the initial concentration which we attribute to effects of the curvature of the solubility curve.

1. Introduction

Room temperature solution methods have numerous advantages for the preparation of nanoparticles. In addition to the less rigorous instrumentation needed for synthesis, the preparation conditions are well suited to many types of materials, in particular organic molecules, which have poor stability at extremes of temperature and pressure. Besides the importance for technological applications, there is considerable interest in understanding the underlying process of molecular self-organization often used to form the nanoparticles. There is a close relation between this self-organization and that occurring in solution crystallization and in many naturally occurring processes.

One method of inducing molecular self-organization relies on a rapid reduction in solubility. This is often accomplished by the addition of a miscible nonsolvent to a solution, placing the solution in a highly supersaturated and often inhomogeneous state. This method is known under various names as reprecipitation,[1] solvent shifting,[2] micronization,[3] or drowning out crystallization.[4] Following the addition of the nonsolvent, a complex process of nuclei formation and growth ensues, resulting eventually in the precipitation of a bulk phase of the solid in equilibrium with a saturated solution. In this process, the system frequently passes through a state in which the solid phase is in the form of a dispersion of nanoparticles suspended in the solvent. The utility of this method for forming nanoparticles lies in the fact that the nanoparticle dispersions are frequently metastable for long periods of time, can be stabilized with the addition of surfactants, and have a high degree of monodispersity.[5−8]

This rapid method of nanoparticle formation has been developed for several applications. A major industrial use of the method is for the production of nanoparticles dispersions of β-carotene and related materials using a process developed by researchers at BASF.[9] This application highlights one advantage of the method: the ability to create stable aqueous nanoparticle dispersions of water-insoluble materials. More recent activity has focused on the preparation of nanosuspensions of drugs, which must be prepared in aqueous formulations but also need to have well-controlled particle sizes and shapes for optimal bioavailability.[10,11]

Nakanishi's group has pioneered the method for use in preparing novel optical and electronic materials.[1] The method has two main advantages here: (i) the ability to create low-scattering nanoparticles of optical materials for which large crystals cannot be easily grown and (ii) the potential enhancement or control of optical properties in nanometer-sized particles through quantum mechanical effects. They have created dispersions of a number of organic nanocrystals, including polydiacetylene,[12] J-aggregates of merocyanine dye,[13] and phthalocyanine nanocrystals.[14] Other groups have adapted the method for preparing nanocrystals of similar materials, such as pyrzolines,[15] porphyrins,[16] tetracene,[17] and a number of other dyes.[18,19] We have been using the solvent shifting method to study nucleation and growth of nanoparticles of model systems of molecular crystals naphthalene[20] and anthracene[21] and, more recently, polymer nanoparticles.[22]

* Corresponding author: Tel, 202-687-5982; e-mail, vankeu@physics.georgetown.edu.

(1) Kasai, H.; Nalwa, H.; Oikawa, H.; Okada, S.; Matsuda, H.; Minami, N.; Kakuta, A.; Ono, K.; Mukoh, A.; Nakanishi, H. *Jpn. J. Appl. Phys.* **1992**, *31*, L1132–L1134.
(2) Texter, J. *J. Dispersion Sci. Technol.* **2001**, *22*, 499–527.
(3) Horn, D.; Rieger, J. *Angew. Chem., Int. Ed.* **2001**, *40*, 4330–4361.
(4) Davey, R. In *Crystal Growth in Science and Technology* Arend, H., Hullinger, J. , Eds.; NATO ASI Series B, Physics, Vol. 210; Plenum Press, New York, 1989; pp 217−224.
(5) LaMer, V.; Dinegar, R. *J. Am. Chem. Soc.* **1950**, *72*, 4847–4854.
(6) Reiss, H. *J. Chem. Phys.* **1951**, *19*, 482–487.
(7) Sugimoto, *Adv. Colloid Interface Sci.* **1987**, *28*, 65–108.
(8) Matijevic, E. *Langmuir* **1994**, *10*, 8–16.
(9) Horn, D. *Angew. Makromol. Chem.* **1989**, *166/167*, 139–153.
(10) (a) Schubert, M.; Müller-Goymann, C. *Eur. J. Pharm. Biopharm.* **2003**, *55*, 125–131. (b) Gassmann, P.; List, M.; Schweitzer, A.; Sucker, H. *Eur. J. Pharm. Biopharm.* **1994**, *40*, 64–72.
(11) *Emulsions and Nanosuspensions for the Formulation of Poorly Soluble Drugs*; Müller, R., Benita, S., Böhm, B., Eds.; Medpharm; Stuttgart; 1998.
(12) Matsuda, H.; Yamada, S.; Van Keuren, E.; Katagi, H.; Kasai, H.; Okada, S.; Oikawa, H.; Nakanishi, H.; Smith, E.; Kar, A.; Wherret, B. *Proc. SPIE* **1997**, *2998*, 241–248.
(13) Matsuda, H.; Van Keuren, E.; Masaki, A.; Yase, K.; Mito, A.; Takahashi, C.; Kasai, H.; Kamatani, H.; Okada, S.; Nakanishi, H. *Nonlinear Opt.* **1995**, *10*, 123–128.
(14) Rangel-Rojo, R.; Matsuda, H.; Kasai, H.; Nakanishi, H. *J. Opt. Soc. Am. B* **2000**, *17*, 1376–1382.
(15) Fu, H.; Yao, J. *J. Am. Chem. Soc.* **2001**, *123*, 1434–1439.
(16) Gong, X.; Milic, T.; Xu, C.; Batteas, J.; Drain, C. *J. Am. Chem. Soc.* **2002**, *124*, 14290–14291.
(17) Kim, H.; Bjorklund, T.; Lim, S.; Bardeen, C. *Langmuir* **2003**, *19*, 3941–3946.
(18) Brick, M.; Palmer, H.; Whitesides, T. *Langmuir* **2003**, *19*, 6367–6380.
(19) Abyan, M.; Bîrlă, L.; Bertorelle, F. ; Fery-Forgues, S. *C. R. Chim.* **2005**, *8*, 127–1281.
(20) Van Keuren, E.; Georgieva, E.; Adrian, J. *Nano Lett.* **2001**, *1*, 141–144.
(21) Van Keuren, E.; Georgieva, E.; Durst, M. *J. Dispersion Sci. Technol.* **2003**, *24*, 721–729.
(22) Van Keuren, E. *J. Dispersion Sci. Technol.* **2004**, *25*, 547–553.

10.1021/la800290s CCC: $40.75
Published on Web 05/15/2008

The similarities between the phenomena underlying this method of nanoparticle synthesis and the processes of solution crystal growth have prompted the application of crystal nucleation theories to describe the nanoparticle formation. Theoretical studies of the thermodynamics of nucleation have a long history, beginning with the works of Gibbs, Volmer, and others,[23] that predict the critical size of clusters above which growth can occur. Below this size, the contributions of surface terms to the particle energy prevent them from growing, even though the solid phase is thermodynamically more stable. The alternate view of nucleation is a kinetic picture, in which the rates of formation of individual species are considered. Most experimental data indicate that heterogeneous nucleation (nucleation induced by impurities or container surfaces) is as important as homogeneous (spontaneous nucleation of clusters), so theories need to include both mechanisms for realistic description of nucleation and growth.[21]

In many thermodynamic descriptions of crystal nucleation and growth a constant level of saturation is assumed; however, in the reprecipitation method the system is closed and the level of saturation changes significantly. The decrease in saturation as nuclei form provides a feedback mechanism for limiting the particle size: as particles grow, the saturation level decreases, reducing the driving force for further growth.[20,21] This phenomenon was described in early models of particle formation developed by LaMer and Dinegar.[5] They surmised that the dependence of the nucleation rate on the concentration above saturation is the key to obtaining narrow size distributions. A steep increase in nucleation rate implies a rapid burst of nucleation above a certain threshold. The formation of stable nuclei will result in a drop in the bulk solution concentration of solute and a corresponding large decrease in further nucleation. The primary particles formed in the initial nucleation will grow by diffusion of molecules to the particle surfaces. The short time period over which the nucleation occurs yields a narrow size distribution of nucleation sites. Furthermore, Reiss showed that the process of diffusional growth will further sharpen particle size distributions.[6] Finally, the phenomenon of Ostwald ripening also narrows size distributions; it occurs due to the lower surface tension in smaller particles, resulting in larger particles growing at the expense of smaller ones.[23] During later stages, though, more recent work by Matjevic's group has shown that the growth is more complex than the simple models predict.[24]

While a large amount of theoretical work has been done to analyze nucleation and crystal growth, there have been fewer experimental studies, in particular in connection with the early stage of solution crystallization. This is partly due to the lack of suitable experimental methods for the time and length scales that need to be probed. A number of studies have demonstrated the existence of prenucleating clusters in supersaturated solutions using measurements of molecular diffusivity,[25] concentration gradients,[26] and various optical techniques.[25,27–29]

An understanding of the growth mechanisms is critical to the development of the technology for producing these nanoparticles. Here we report on quantitative studies of the self-organization of magnesium phthalocyanine (MgPC) during reprecipitation to form nanoparticles. The phthalocyanines are a class of cyclic molecules, often ligated to central metal ions. Besides the considerable interest in phthalocyanines and the related porphyrins because of their similarity to hemoglobin and chlorophyll, they have considerable technological uses, including data storage and optical displays.[30] We are specifically interested in studying these materials for two reasons. One is that the formation of dimers and larger *n*-mers is typically accompanied by significant changes in the optical spectra, including shifts and appearance of new bands in the absorption, and strong quenching of fluorescence in the emission spectra. A second reason is that the phthalocyanines and porphyrins have shown themselves to be suitable for nanoparticle formation using reprecipitation.[16,31,32]

The single molecule MgPC has a slightly off-planar shape with the Mg atom shifted away from the plane of the macrocycle.[33] As a crystal, it may exist in several forms. In addition to the α and β forms common to most phthalocyanines,[34] a crystalline phase displaying a strong infrared absorption band, denoted the X-phase, has also been observed.[35] This phase has been identified as aquamagnesium phthalocyanine, a complex of the phthalocyanine and water, with the new absorption band arising due to interactions between the phthalocyanine molecules.[36,37] The infrared peak characteristic of this phase has been observed in MgPC solutions in DMF/water by Sapunov,[32] as well as in benzonitrile/water.[37] Sapunov used a kinetic analysis to attribute the near-infared (NIR) band to the formation of the MgPC trimer. In addition to the changes in the absorption spectra, MgPC shows strong fluorescence quenching in both dimers and in the X-phase.[38]

We use these changes in the optical properties that occur on self-organization as a measure of the state of the molecules in solution, along with the change in size of growing particles obtained from photon correlation spectroscopy (PCS) measurements in order to study the growth of the nanoparticles. The decrease in the fluorescence as a function of time is proportional to the decrease in the number of single, isolated molecules remaining in solution. If particles grow by the diffusion of these single molecules to their surfaces and the subsequent attachment, the rate of their removal from solution should be correlated to the rate of the growth in particle size. If the growth mechanism is aggregation of smaller primary particles, the rates should be different: the decay rate of fluorescence will indicate the growth rate of primary particles (< 10 nm), while the particle sizes found from PCS will correspond to the primary particles aggregating. By measuring these quantities simultaneously, we are able to correlate these two phenomena and obtain validation of specific growth models. We present results from studies of the self-organization as a function of time after mixing.

2. Experimental Section

2.1. Sample Preparation. Magnesium phthalocyanine (Fisher Scientific) was purified by recrystallization from methanol. Solutions

(23) Nývelt, J. *Cryst. Res. Technol.* **1995**, *30*, 443–449.
(24) Park, J.; Privman, V.; Matijevic, E. *J. Phys. Chem. B* **2001**, *105*, 11630–11635.
(25) (a) Myerson, A.; Lo, P. *J. Cryst. Growth* **1990**, *99*, 1048–1052. (b) Mohan, R.; Kaytancioglu, O.; Myerson, A. *J. Cryst. Growth* **2000**, *217*, 393–403.
(26) Mullin, J.; Leci, C. *Philos. Mag.* **1969**, *19*, 1075–1077.
(27) (a) Izmailov, A.; Myerson, A.; Arnold, S. *J. Cryst. Growth* **1999**, *196*, 234–242. (b) Na, H.; Arnold, S. ; Myerson, A. *J. Cryst. Growth* **1994**, *139*, 104–112.
(28) Tamagawa, R.; Miranda, E.; Berglund, K. *Cryst. Growth Des.* **2002**, *2*, 263–267.
(29) Pasternack, B.; Collings, P. *Science* **1995**, *269*, 935–939.
(30) McKeown, N., *Phthalocyanine Materials*; Cambridge University Press: Cambridge, 1998.
(31) Rangel-Rojo, R.; Yamada, S.; Matsuda, H.; Kasai, H.; Komai, Y.; Okada, S.; Oikawa, H.; Nakanishi, H. *Jpn. J. Appl. Phys., Part 1* **1999**, *38*, 69–73.
(32) Sapunov, V. *Russ. J. Phys. Chem.* **2002**, *76*, 1221–1227.
(33) Fisher, M.; Templeton, D.; Zalkin, A.; Calvin, M. *J. Am. Chem. Soc.* **1971**, *93*, 2622–2628.
(34) Janczak, J.; Kubiak, R. *Polyhedron* **2001**, *20*, 2901–2909.
(35) Hor, A.; Loufty, R. *Thin Solid Films* **1983**, *106*, 291–301.
(36) Endo, A.; Matsumoto, S.; Mizuguchi, J. *J. Phys. Chem.* **1999**, *103*, 8193–8199.
(37) Janczak, J.; Idemori, Y. *Polyhedron* **2003**, *22*, 1167–1181.
(38) Phillips, D.; Dhami, S.; Ostler, R.; Petrasek, Z. *Prog. React. Kinet. Mech.* **2003**, *28*, 299–420.

were prepared in spectroscopic grade acetone (Acros) and degassed with dry nitrogen. Nanoparticles were prepared by rapidly mixing the MgPC solutions and distilled−deionized water, also degassed. Unless noted otherwise, this mixing was accomplished by injecting the water into the MgPC solutions with an 18 gauge pipetting needle immersed into the center of the sample vial. All preparation was carried out at room temperature, which was confirmed for each measurement to be 25 ± 1 °C. Unless otherwise noted, the initial concentration of the MgPC in acetone was 10 μM and the rate of injection was approximately 1.0 mL/s. We relied on the rapid injection for mixing the solvents; following the injection, no additional stirring was done, and further mixing was through residual convection and solvent diffusion.

2.2. Characterization. The formation of the MgPC nanoparticles was characterized by photon correlation spectroscopy (PCS), fluorescence emission, and UV−vis spectroscopy. In PCS, a standard particle sizing method, temporal fluctuations of the scattered light due to particle motion (e.g., diffusion) are characterized through calculation of the time-autocorrelation function of the scattered signal.[39] From these, particle size information can be determined using the relation between the diffusion coefficients and the size and shape of the particles.

Our PCS setup is assembled from discrete optical components. The incident beam was emitted by a high-performance 10 mW HeNe laser with wavelength 632.8 nm (JDS Uniphase). The beam was incident on the sample in a 1 cm^2 cross section sample cuvette. Light scattered at 90° to the incident beam was collected by a single mode optical fiber. Single mode fibers have been shown to be ideal for collecting scattered light in PCS experiments, since they have high efficiency for coupling light and the fact that they are single mode guarantees that the measured signal is spatially coherent, optimizing the signal-to-noise ratio of the autocorrelation function.[40] In most of the time-dependent measurements, the signal was sampled for 15 s in order to provide good statistics for calculation of the radii.

The fiber was connected to a photon counting avalanche photodiode (EG&G), whose signal was processed by an ALV5000 (ALV GmbH, Germany) hardware autocorrelator. The data were analyzed using the method described by Frisken,[41] which directly uses the autocorrelation function (not its square) and takes into account an arbitrary background signal. Nonlinear fits were performed of the autocorrelation data to the function

$$g_2(\tau) = \beta e^{-2\Gamma\tau}\left(1 + \frac{\mu_2}{2!}\tau^2 - \frac{\mu_3}{3!}\tau^3\right)^2 + B \qquad (1)$$

where β is a factor that depends on the experimental geometry (coherence area of detector), Γ, μ_2, and μ_3 are the first, second, and third moment of the distribution of decay times, and B is a background term. Since most of the data were close to monoexponential functions of the decay time, inclusion of the third moment in the fitting had negligible effect and was normally set to zero. The second moment, μ_2, is a measure of the width of the distribution and was used to calculate the dimensionless polydispersity index (PDI):

$$\mathrm{PDI} = \mu_2 / \Gamma^2 \qquad (2)$$

A PDI of zero implies a monoexponential decay to the autocorrelation function, which in turn signifies a single diffusion coefficient.

From the fit results, the scatterer diffusion coefficients and polydispersity indices (relative width of the particle size distributions) were found. The Stokes−Einstein equation, along with the viscosity of the water/acetone solvent mixture,[42] was used in order to determine the corresponding hydrodynamic radii from the decay times. The instrument accuracy was checked with polystyrene microsphere standards.

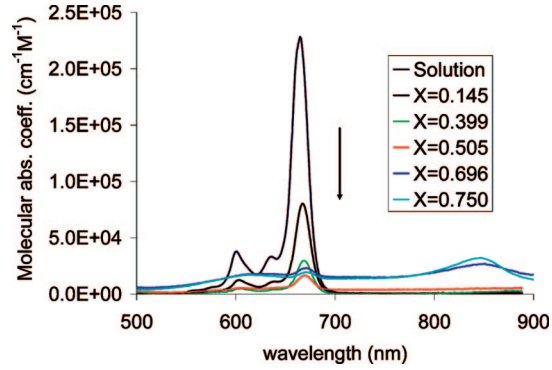

Figure 1. MgPC molar absorption coefficient for various mole fractions of added water.

The UV−vis absorption and fluorescence emission spectra were measured with minispectrometers (Ocean Optics Chem2000). For absorption spectra, a deuterium tungsten light source was used and the spectra were measured between 190 and 890 nm with a resolution of 0.3 nm. For the fluorescence emission, the sample was excited with the same HeNe laser as used for PCS experiment; the wavelength is close to the absorption maximum of MgPC in solution (665 nm). The emission between 650 and 900 nm was coupled into an optical fiber and input into the spectrometer. The beam path through the sample was positioned near the edge of the cuvette in order to minimize reabsorption of the fluorescence emission by the dye solution. Fluorescence emission and PCS were performed simultaneously using the same incident laser beam, with both fibers aligned at 90° with respect to the beam direction. The ability to perform these two separate measurements simultaneously enables us to accurately correlate the time dependence of the particle growth with the fluorescence changes in the solution.

While concentration and temperature were constant in each of the experiments, the mixing process could not be precisely controlled, leading to some variations from run to run. At each concentration presented in the following sections, at least four independent runs were carried out in order to determine the statistical variations in the results of the fitting procedure. As shown later in section 3.4 (Figure 7), the variation in the particle sizes from PCS measurements ranged from 7% to 30%. In order to assess the effects of permanent photobleaching, we repeated the time-dependent data shown later at only a few times after mixing. Between measurements, the excitation beam was blocked. No noticeable changes were observed in the results.

3. Results and Discussions

3.1. UV−vis Absorption. The effect of the solvent on the absorption spectra is shown in figure 1. With the addition of the nonsolvent, the MgPC self-organizes to form nanoparticles. The optical absorption spectra of these particles are dramatically different from that of the isolated molecule. Molecular MgPC displays characteristic spectra of phthalocyanines:[30] a broad Soret band absorption centered around 345 nm (not shown in figure) and a strong sharp peak around 665 nm, the Q-band. While the Soret band is relatively insensitive to the molecule's surroundings, the Q-band, attributed to a $\pi-\pi^*$ transition in the macrocycle, depends strongly on the environment.[30]

The figure shows the spectra for MgPC in acetone and in a range of acetone/water binary solvents with different ratios of the two solvents. The spectra were measured 1.5 h after mixing the solvents, allowing sufficient time for the particles to form. The strong Q-band is initially red-shifted, possibly due to the

(39) (a) Berne, B.; Pecora, R. *Dynamic light scattering: with applications to chemistry, biology, and physics*; R.E. Krieger Pub. Co.: Malabar, FL, 1990. (b) Chu, B. *Laser light scattering: basic principles and practice*; Academic Press: Boston, 1991.
(40) Rička, J. *Appl. Opt.* **1993**, *32*, 2860–2875.
(41) Frisken, B. *Appl. Opt.* **2001**, *40*, 4087–4091.
(42) Noda, K.; Ohashi, M.; Ishida, K. *J. Chem. Eng. Data* **1982**, *27*, 326–328.

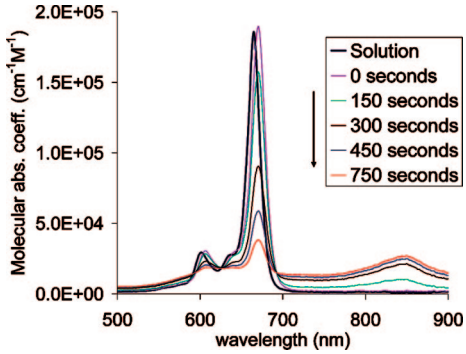

Figure 2. Molecular absorption coefficient vs time after solvent mixing for a sample with a mole fraction of water $X = 0.696$.

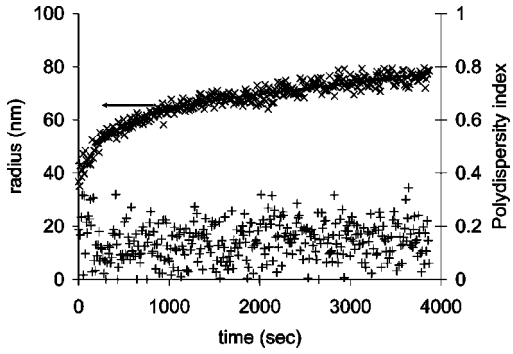

Figure 3. Particle radius and polydispersity index vs time for a mole fraction of water = 0.535 (×, measured radius; solid line, fitted radius; +, PDI).

change in the solvent polarity or the association of water molecules with the MgPC molecules. Then it decreases as the mole fraction of water is increased. Along with this, the infrared band centered around 840 nm appears and grows with increasing water content. In addition, there is the appearance of a relatively flat background due to scattering. At still later times, several hours to days depending on the mole fraction of water, large aggregates are visible settling out of solution and the entire spectra decreases. The Soret band shows little change with increasing water content.

Figure 2 shows the time dependence of these changes in the spectra for a 0.696 mol fraction of water. The changes in time mirror those show in Figure 1 for the concentration dependence. At this concentration, the Q-band shifts and then decreases rapidly within tens of minutes, while the NIR band increases. There is an isobestic point at wavelength 694 nm which would indicate only two species with different absorption properties. At lower water mole fractions, the decay of the Q-band is not complete (it does not completely disappear) and the growth of the NIR band is weak or not seen at all.

3.2. Particle Size versus Time. The changes in the absorption spectra occur due to the isolated molecules in solution associating with other molecules or nanoparticles. Figure 3 shows the results of the PCS measurements of the particle hydrodynamic radius versus time for one sample. As observed in our earlier work,[20] there is a rapid growth in the particles at short times on the order of tens to hundreds of seconds. The growth then slows as the molecules in solution are depleted.

Rather than assuming a specific model of particle growth to analyze the data, we fit an empirical relation to the radii in order to extract the characteristic sizes and time scales. In most of the data, the particle size shows a rapid initial growth which then

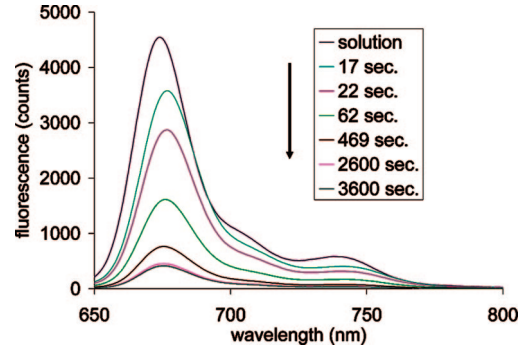

Figure 4. Fluorescence spectra of the solution and the nanoparticle dispersions for various times after mixing for a mole fraction of water = 0.535.

levels off to an almost linear increase versus time. We use a function of the form

$$r(t) = r_0 + a(1 - e^{-t/\tau}) + r_L t \quad (3)$$

where r_0 is the initial radius at zero time, a is a normalization, τ is a characteristic time for the particle growth, and r_L is the coefficient of slower linear growth that dominates at later times. Due to the need to sample the signal for PCS for times on the order of tens of seconds in order to obtain statistically good data, the measurements miss the rapid initial particle formation occurring at times of a few seconds or less; the initial radius term r_0 accounts for this formation. The fitted function is also shown in Figure 3 for those data.

Also shown in the figure is the polydispersity index (PDI) for these data. The relatively small values of the PDI imply a narrow distribution of particles sizes about the mean radius. As described earlier, the narrow distribution of particle sizes is characteristic of this method of nanoparticle formation.

These results conform to earlier studies of particle growth using this method, namely, rapid nucleation of particles on time scales shorter than can be observed with PCS (several seconds), then growth of these primary particles, followed by slower growth as these aggregate. What is not clear from the PCS measurements is how the growth of the primary particles occurs. However, the simultaneous measurement of the fluorescence emission enables the correlation of the decrease in monomer concentration with the growth in the particle size.

3.3. Fluorescence Quenching. Figure 4 shows the fluorescence emission spectra for a 10^{-5} M solution of MgPC along with the emission at several times after the addition of 0.55 mL water to a 1.95 mL solution (water mole fraction 0.535).

The use of the HeNe laser as the excitation source results in an additional decrease in fluorescence due to the decrease in absorption at 632.8 nm from monomers to dimers, which gives a less efficient excitation. This increases the effect of the fluorescence quenching in the nanoparticles. The quenching was also observed in spectra in which the UV bands from a mercury lamp were used as excitation source instead of the HeNe laser. The overall decrease in the emission is due to both fluorescence quenching in the dimer and larger aggregates as well as the decrease in the absorption coefficient at the excitation wavelength.

The time scales for fluorescence decay and particle growth show notable differences in all cases. Assuming the emission is due to the unassociated monomers remaining in solution, the decrease in the emitted fluorescence signal ($S_F(t)$) from its initial value (S_0) should be proportional to the total number of solute

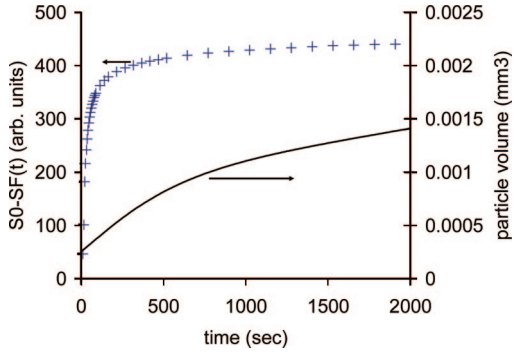

Figure 5. Change in integrated fluorescence emission and particle volume vs time for a mole fraction of water = 0.535 (+, fluorescence change; solid line, particle volume).

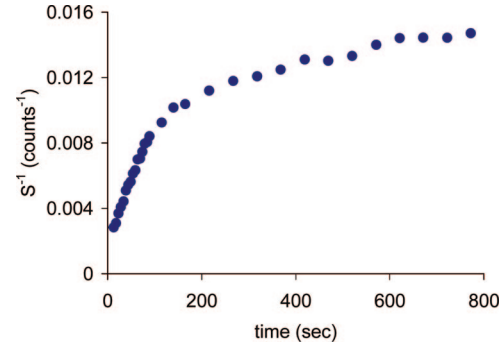

Figure 6. The inverse of the integrated fluorescence emission ($1/S$) vs time after mixing for a sample with mole fraction of water = 0.563.

molecules in particles, which will in turn be proportional to the particle volume

$$S_0 - S_F(t) \propto \sum n_i(t)V_i(t) = V(t) \tag{4}$$

where the equality holds for a monodisperse sample. Figure 5 depicts a typical example of the time-dependent volume change, calculated from the fit of eq 3 to the r versus time data, along with the change in fluorescence. The two curves have markedly different time scales, i.e., do not follow the form of eq 4. This provides further confirmation of the arguments of Park et al.[24] and Kasai et al.[43] that the growth in these systems at these time scales is not monomer diffusion to the surfaces of the growing particles. However, the slow decrease in fluorescence even at longer times does imply that the attachment of monomers to other monomers or growing particles is an important part of the growth. We are currently applying growth models that include the effect of cluster distributions[44] to the results presented here.

Assuming that the fluorescence originates from monomers only, the main initial mechanism for reducing the number of monomers will be dimerization. In a homogeneous system, the rate of change of the monomer concentration will be proportional to the square of the concentration

$$\frac{dx}{dt} = -kx^2 \tag{5}$$

where x is the monomer concentration ($x = x(t)$) and k is the rate of dimerization. The solution is

$$x(t) = \frac{x_0}{1 + x_0kt} \tag{6}$$

where x_0 is the concentration at $t = 0$. Assuming the fluorescence is proportional to the monomer concentration

$$S(t) = cx(t) \tag{7}$$

then

$$\frac{1}{S(t)} = \frac{1}{cx(t)} = \frac{1 + x_0kt}{cx_0} = \frac{1}{cx_0} + \frac{kt}{c} \tag{8}$$

The plots of $1/S(t)$ showed a high degree of linearity with time at short times, as seen in Figure 6, suggesting that dimerization remains an important mechanism in the nanoparticle growth in the early stages, despite the fact that the mixture is highly inhomogeneous. A fit of eq 8 to the early time data was used to determine the dimerization rates; however, no correlation to the particle growth parameters found from the light scattering could be observed.

3.4. Growth Dependence on Concentration. For practical applications, the influence of various preparation conditions on the resulting nanoparticle growth needs to be identified. Kasai et al. found a sensitive dependence of the growth on the temperature of the system in nanoparticles of perylene prepared in a similar process.[43] We investigated the concentration dependence of the parameters found from fits of eqs 3 and 8 to the PCS and fluorescence data, respectively. In particular, we varied the ratio of solvents (mole fraction of water) while keeping the total sample volume constant.

As might be expected, there was some variation in results among experiments at identical concentrations, due to the inexact nature of the mixing process. However, the fitted results were relatively reproducible and several trends could be observed as a function of concentration.

While the time dependence of the particle growth varied significantly from run to run, it surprisingly did not show any systematic dependence on the mole fraction of water. One would expect some dependence both due to the change in the total concentration of MgPC in the binary solvent (since the initial concentration of the MgPC in acetone remained constant, the concentration in the mixed solvent changes) and from the different amounts of initial supersaturation. In addition, while the details of the particle formation are likely sensitive to the heterogeneities formed during mixing, we found no systematic dependence of any of the particle growth parameters on the injection rate in the range 0.1−1.0 mL/s.

The only significant concentration dependence observed was in the primary particle size as a function of water volume fraction. Figure 7 shows the primary particle radius ($r_0 + a$) versus the mole fraction of water for an initial concentration of 10^{-5} M MgPC in acetone. The total volume of the mixture was kept constant. In this model, the quantity $r_0 + a$ represents the average particle size after the initial growth stage. The PDI followed a similar trend, with a value of approximately 0.2 for small and large mole fractions and increasing to >0.5 in the region around $X = 0.7$.

A possible explanation for this lies in the curvature of the solubility curve. The constant volume condition for the mixture gives a straight line across the ternary phase diagram of Figure 8, while the solubility curve is typically curved as shown.[45] In the intermediate region of the diagram the difference between the curves is larger, meaning that the level of supersaturation will be higher. In closed systems in which the supersaturation varies due to nucleation of a solid phase, Slezov et al. have

(43) Kasai, H.; Oikawa, H.; Okada, S.; Nakanishi, H. *Bull. Chem. Soc. Jpn.* **1998**, *71*, 2597–2601.
(44) Madras, G.; McCoy, B. *J. Cryst. Growth* **2006**, *286*, 131–136.
(45) Masing, G. *Ternary Systems*; Dover: New York, 1960.

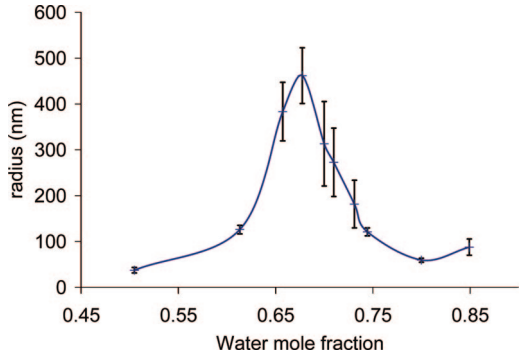

Figure 7. Radius of primary particles vs mole fraction of added water (the line is drawn as a guide to the eye).

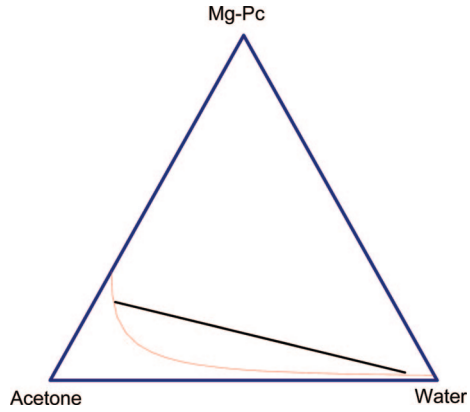

Figure 8. Ternary phase diagram for MgPC in acetone/water. The lower curved line is the solubility curve and the upper straight line shows the water volume fractions from Figure 7. (The MgPC concentrations values have been amplified for better viewing; both curves are actually very close to the bottom axis.)

shown that the sizes of the particles will depend on the initial level of supersaturation.[46] This implies a particle size that will be small near the ends of the solubility curve, where it intersects with the line showing the volume fractions used in the measurements of Figure 7, and large in the center, where there is a much higher level of supersaturation.

4. Conclusions

By correlating simultaneous measurements of the fluorescence decay and particle growth profiles, we have been able to corroborate specific models of particle growth. Once nuclei have formed, the primary mechanism of further particle growth is not molecular diffusion to nuclei surface. Instead, the much more rapid drop in fluorescence emission implies that molecular association occurs at a much faster rate than the increase in particle sizes. The growth could be due to Ostwald ripening, as molecules from smaller particles desorb in favor of attachment to larger particles. The lack of change in the polydispersity index, though, does not corroborate this—one would expect a narrowing of a broader size distribution over time from Ostwald ripening. However, it is reasonable if we include the population of clusters, which are too small to be observed in the light scattering experiments. As described earlier, the rapid nucleation of primary particles after mixing will quickly put the mixture in the metastable region of the phase diagram. Here the unstable clusters will form, quenching the fluorescence, but will not be stable enough to become growing particles. They, along with the molecules remaining in solution, will serve as sources for the growth of the stable primary nuclei formed initially.

Drain et al. reported qualitative indicators that the particle formation is dictated by both kinetic and thermodynamic effects in porphyrin nanoparticles prepared in a similar manner as those reported here.[47] In other studies of solution growth of organic and inorganic nanoparticles in which supersaturation is induced by different methods, similar effects are also observed, i.e., there is evidence of rapid association of molecules followed by stable growth of some fraction of these. Erdemir found the coexistence of *n*-mers with monomers in undersaturated solutions of glycine and above saturation, initial quick dimerization stage followed by nucleation at a later stage.[48] Likewise, simulations of the growth of protein crystals have indicated rapid formation of tetramers as stable complexes, with only a small fraction of these reaching a larger critical radius at a later stage in the growth.[49] Tiemann et al. used stopped flow spectroscopy to demonstrate the predominant role of ripening in the solution growth of ZnS nanoparticles.[50] In these and other studies, the growth of stable particles typically follows a similar pattern of rapid initial increase in particle size that plateaus as the supersaturation is reduced.[48,50,51]

We have also observed an unexpected dependence of the particle sizes on the mole fraction of the water (or the ratio of components of the binary solvent), which we attribute to the curvature of the solubility curve, although more work is needed to confirm this. While this model is yet to be confirmed, the dependence does give an empirical handle on control of the particle size.

Acknowledgment. This material is based upon work supported by the National Science Foundation under Grant No. DMR-0348955 and a Grant-in-Aid from the Cosmos Club of Washington, DC.

LA800290S

(46) Slezov, V.; Schmelzer, J.; Tkatch, Y. *J. Chem. Phys.* **1996**, *105*, 8340–8351.

(47) Drain, C.; Smeureanu, G.; Patel, S.; Gong, X.; Garno, J.; Arijeloye, J. *New J. Chem.* **2006**, *30*, 1834–1843.

(48) Erdemir, D.; Chattopadhyay, S.; Guo, L.; Ilavsky, J.; Amenitsch, H.; Segre, C.; Myerson, A. *Phys. Rev. Lett.* **2007**, *99*, 115702.

(49) Kierzek, M.; Pokarowski, P.; Zielenkiewicz, P. *Biophys. Chem.* **1999**, *77*, 123–137.

(50) (a) Tiemann, M.; Wei, Ö.; Hartikainen, J.; Marlow, F.; Lindén, M. *ChemPhysChem.* **2005**, *6*, 2113–2119. (b) Tiemann, M.; Marlow, F.; Beieler, F.; Lindén, M. *J. Phys. Chem.* **2006**, *110*, 23142–23147.

(51) Fan, W.; O'Brien, M.; Ogura, M.; Sanchez-Sanchez, M.; Martin, C.; Meneau, F.; Kurumada, K.; Sankar, G.; Okubo, T. *Phys. Chem. Chem. Phys.* **2006**, *8*, 1335–1339.